Chapter 1 Introduction

1.1 Introduction of the nanotechnology

Nanotechnology is the creation of functional materials, devices, and systems with the nanometer (1 to 100 nm) length scale. These would result in much novel properties and phenomena in the Chemistry, Physics, Electronics, and Optics …etc. The nanometer length scale also means the more components and functions could be integrated into a smaller device to create the more applications. To create the structure of nanometer length scake there are two major aspects: “top-down” and “bottom-up” fabrication techniques as shown in Fig.1-1.

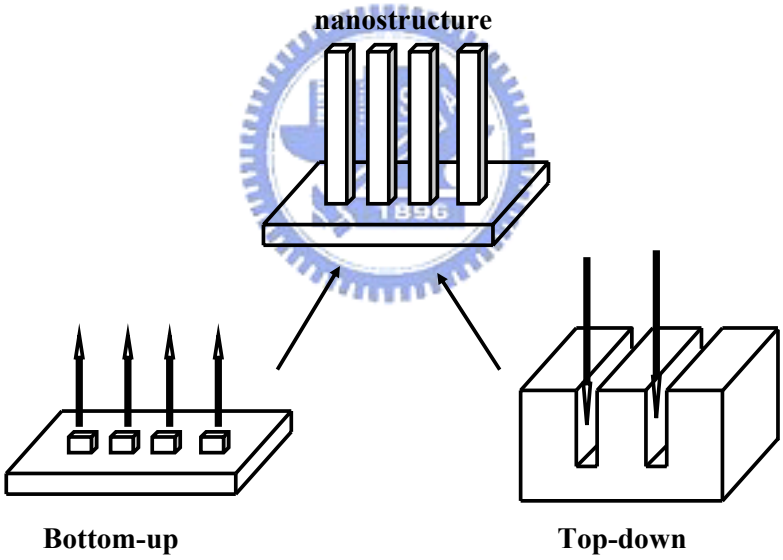

Fig. 1-1. Diagram of top-down and bottom-up.

The techniques of the top-down aspect have been developed for a long time and used enormously in traditional and semiconductor industry such as ultraprecision machining, micro lithography……etc. It has encountered some difficulty to further approach to the nanostructure. Fig. 1-2 shows that the bottom-up method have attracted more and more research attention on making up the nanostructure in the

recent years. One-dimension semiconductor nanostructure such as nanowires, nanotubes, nanobelts, and nanosprings[1~4] have been fabricated by the bottom-up methods such as: chemical vapor deposition (CVD), laser ablation, vapor phase evaporation, and solution and template based methods.[5~9] Through these methods, the selected materials will be fabricated by the following mechanisms: vapor-liquid-solid (VLS)[6], solution-liquid-solid (SLS)[8], and vapor phase epitaxy[7].

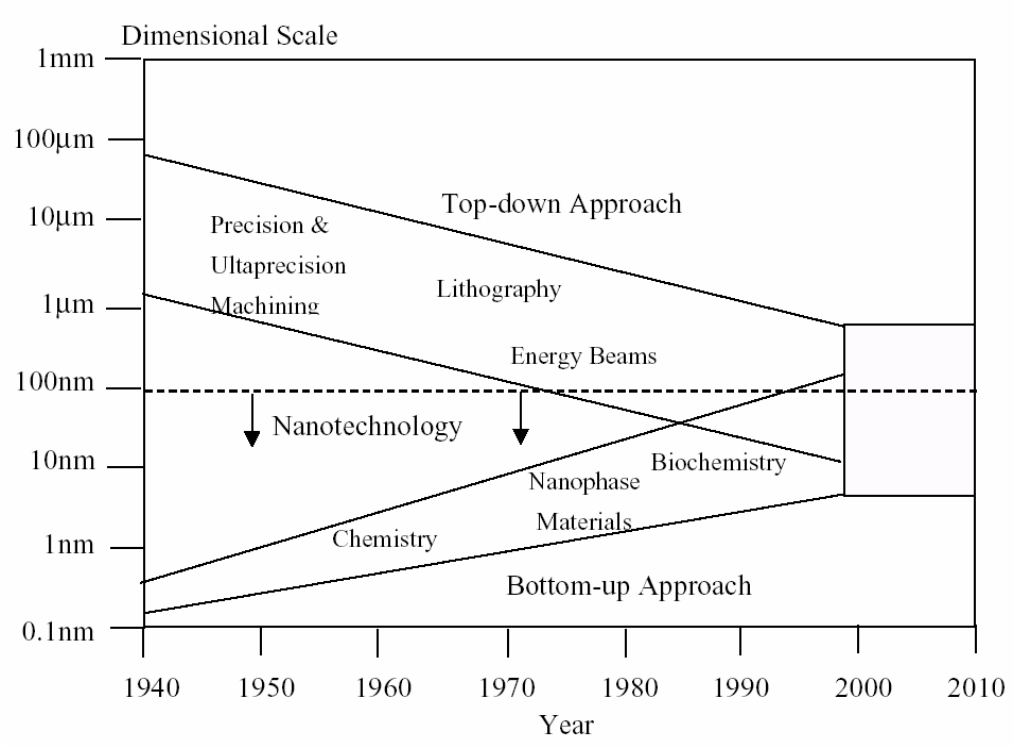

Fig. 1-2.The development tendency of minimum process

Many applications of the semiconductor nanostructures have been developed such as the nano-logic gate (Fig. 1-3 (a)) and nano-laser source (Fig. 1-3 (b)).

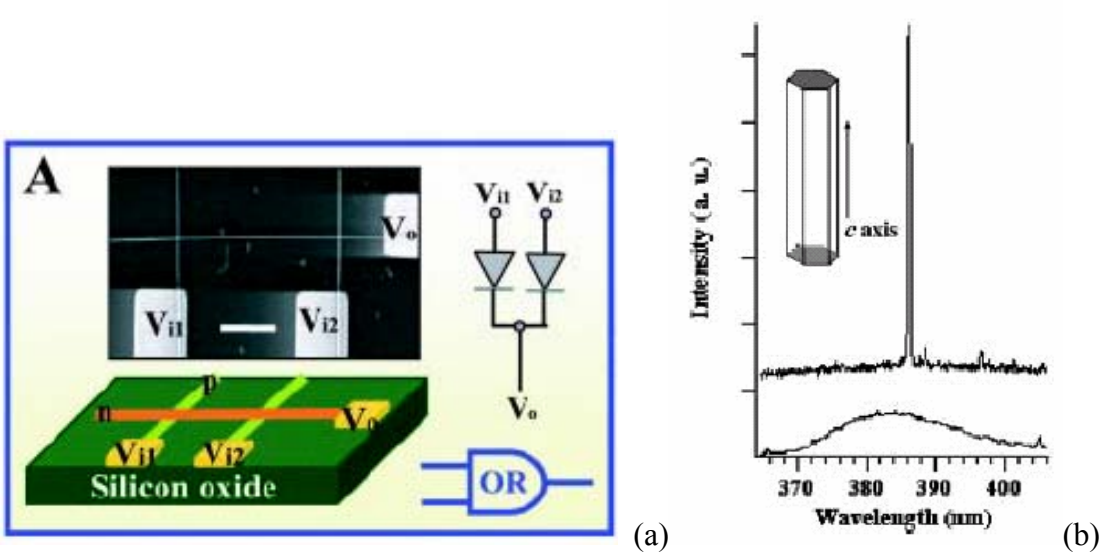

(a) (b)

Fig. 1-3 (a) The nano-logicgate is made by assembled Si nanowires.[14] (b) The nano-laser source makes of the ZnO nanowires.[1]

1.2 Properties of the ZnO

Zinc oxide is a wide band gap (3.37eV) semiconductor material, for which ultraviolet lasing action has been reported in disordered particle and thin films.[10~12] In this regard, ZnO is a good candidate for room temperature UV lasing as its exciton binding energy is approximately 60 meV, significantly larger than that of ZnSe (22 meV) and GaN (25 meV).

1.3 The Review of the ZnO nanostructures

Recently, many groups had grown ZnO nanowires on sapphire and silicon by simple vapor transport and condensation process via vapor-liquid-soild mechanism or by MOVPE via vapor-solid mechanism.[7,13] The more complicated nano-structure of the ZnO were fabricated and found for other object. To investigate the formation mechanism of ZnO on the nano-length scale, the ZnO nanohelixes were discussed in Ref. 4. The inverse ZnO structure and the periodic nanowire array were made for studing the photonics properties.

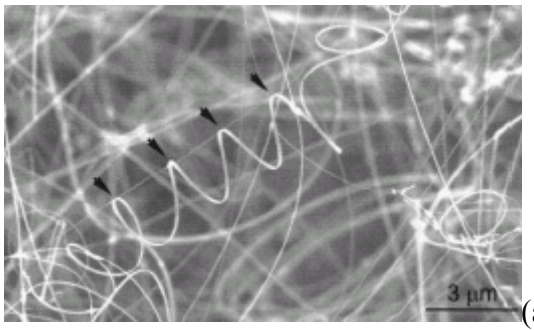

(a)
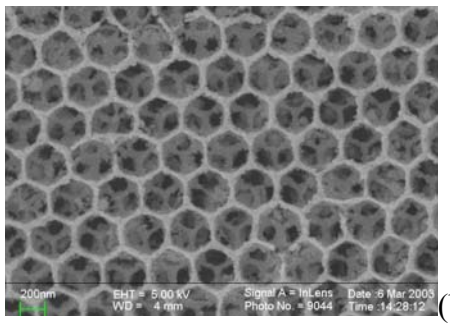

(b)
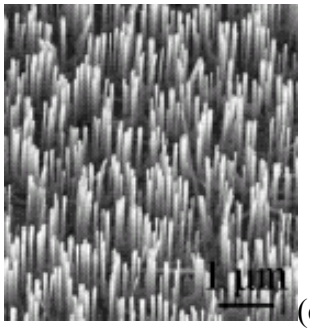

(c)

Fig.1-4 (a) The nano-spring[4] (b) the inverse structure[15] (c) the periodic ZnO nanowires array.[16]

The Peidong Yang's group had demonstrated the lasing research of the ZnO nanowires in Ref. 1 and 17. Through optical pumping method the ZnO nanowires array and single nanowire showed UV lasing in the spectra. (Fig. 1-3(b)) These researches revealed the potential of the ZnO nanowires for laser source and a new laser diode.

1.4 Motivation

The ZnO material has a very high UV emission efficiency at room temperature and the UV lasing was observed in the ZnO nanowires for the structure of nanowires. Through the VLS method the ZnO nanowires were grown with catalyst on the top end which complicated the nanowires lasing research. In this study we employ the vapor deposition refer to Ref. 22 to grow the ZnO nanowiers without catalyst on the top end. With well morphology the nanowires are contributive for measuring the relationship between the morphology and the optical properties such as the optical mode inside the nanowires[17]. The vapor deposition method works at 550℃~650℃ much lower than the VLS method with the Au catalyst which worked at about 950℃[21] , and the

as-grown nanowires have well-aligned orientation on the quartz substrate. The lower growing temperature still has high optical quality as compared to the solution method[18]. Without catalyst in the process, the diameters of the nanowiers could be controlled by adjusting the growth pressure.

1.5 Organization of the thesis

Beside this chapter the thesis include other four chapters. In chapter 2 we will exhibit the theories background of the experiments such as the vapor phase epitaxy mechanism, Scanning Electron Microscopy (SEM), Transmission Electron Microscope (TEM), photoluminescence (PL) spectrum, and x-ray diffraction (XRD) spectrum. In chapter 3, we display the experiment details including the measurement apparatus and processes. By means of the SEM, TEM, XRD, and PL spectrum, the morphology, crystalline quality, and optical emission properties of the ZnO nanowires will be investigated and discussed in the chapter 4. Then we made a conclusion in the final chapter.

Chapter 2 Theoretical background

2.1 The mechanism of ZnO nanowires formation

The semiconductor material nanowires can be synthesized by various methods such as hydrothermal process, laser ablation, MOCVD, physical vapor deposition, and vapor-liquid-solid (VLS) methods.[18~22] The processes of making semiconductor nanowires are continually invented in the way of less cost and better crystalline quality for supporting wide applications in electronic and optical region.

The VLS method was originally developed by Wagner and his co-workers to produce micrometer-sized whisker in 1960s.[36] Recently, this technique is re-examined by Lieber, Yang. A typical VLS process starts with the dissolution of gaseous reactants into nanosized liquid droplet of a catalyst metal, and then followed by nucleation and growth of single crystalline nanorods and nanowires. The 1D growth is mainly induced and dictated by the liquid droplets, the size of which remain essentially unchanged during the entire process of nanowire growth. In the sense, each liquid droplet serves as a soft template to limit strictly the lateral growth of an individual nanowire. As a major requirement, there should exist a good solvent capable of forming liquid alloy with the growing material, ideally they should be able to form eutectic compounds. All major steps involved in a VLS process schematically illustrated in Fig. 2-1. Based on the Zn-Au binary phase diagram (Fig. 2-2), Zn and Au form liquid alloys when the temperature is raised above the eutectic point. Once the liquid droplet is supersaturated with Zn, nanowire growth will begin to occur at solid liquid interface. The vapor pressure of Zn in the CVD system has to be kept sufficiently low that second ordinary nucleation events will be completely suppressed. Both physical methods (thermal evaporation, laser ablation) and chemical

methods (chemical vapor transport and deposition) have been employed to generate the vapor species required for the growth of nanowires, and no significant difference was found in the quality of nanowires produced by these methods.

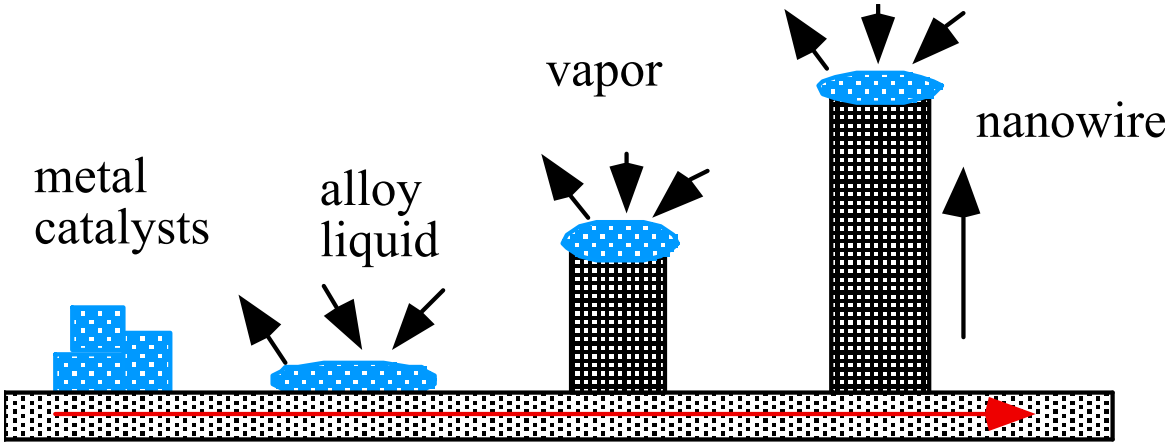

Fig. 2-1 VLS method

Ⅰ : Au-Zn alloying

Ⅱ : ZnO nucleation

Ⅲ : ZnO nanowire growth

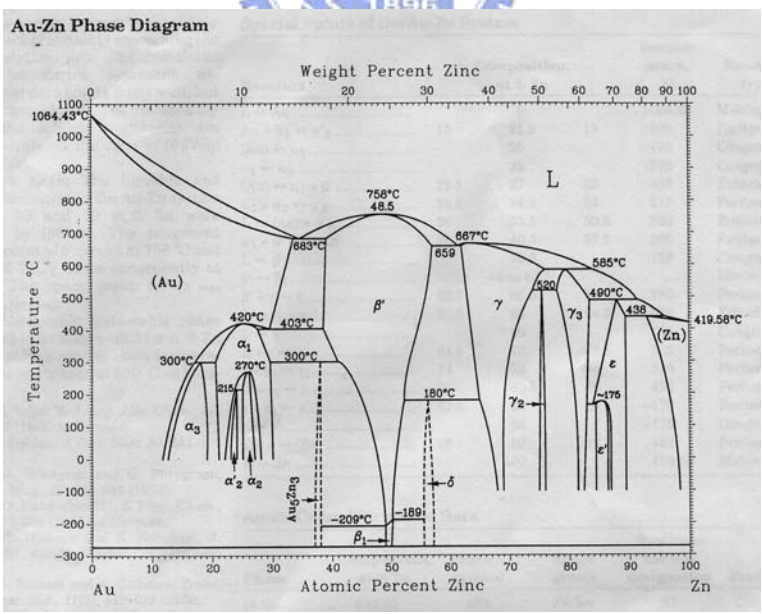

Fig.2-2 Au-Zn phase diagram

In this thesis, the well aligned ZnO nanowires arrays were synthesized by the low temperature vapor deposition method which referred to Ref. 22.

2.2 X-ray diffraction

2.2.1 ω-2θ scan

A crystal consists of a regular array of atoms, each of which can scatter electromagnetic waves. A monochromatic beam of X-rays that falls upon a crystal will be scattered in all directions inside it. However, owing to the regular arrangement of the atoms, in certain directions the scattered waves will constructively interfere with one another while in others they will destructively interfere. The atoms in a crystal may be thought of as defining families of parallel planes, as in Fig. 2-3(a), with each family having a characteristic separation between its component planes. This analysis was suggested in 1913 by W. L. Bragg. The conditions that must be fulfilled for radiation scattered by crystal atoms to undergo constructive interference may be obtained from a diagram like that in Fig. 2-3(b). A beam containing X-rays of wavelength λ is incident upon a crystal at an angle θ with a family of Bragg planes whose spacing is d. The beam goes past atom A in the first plane and atom B in the next, and each of them scatters part of the beam in random directions. Constructive interference takes place only between those scattered rays that are parallel and whose paths differ by exactly λ, 2λ, 3λ, and so on. That is, the path difference must be nλ, where n is an integer. The only rays scattered by A and B for which this is true are those labeled I and II in Fig. 2-3(b).

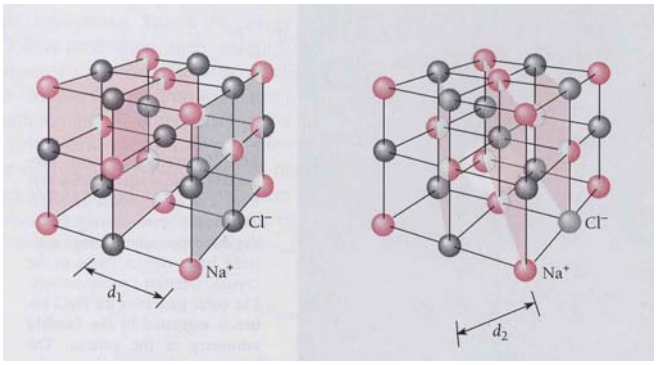

Fig. 2-3(a) Two sets of Bragg planes in an NaCl crystal

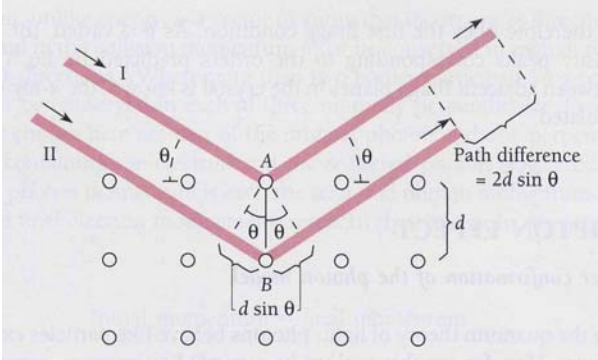

Fig. 2-3(b) X-ray scattering from a cubic crystal

The first condition on I and II is that their common scattering angle be equal to the angle of incidence θ of the original beam. The scond condition is that

$$2d\sin\theta = n\lambda \qquad n = 1,2,3,... \qquad (2\text{-}1)$$

since ray II must travel the distance $2d\sin\theta$ farther than ray I. The integer n is the order of the scattered beam.[37] Then Considering hexagonal unit cell in Fig. 2-4 which is characterized by lattice parameters a and c. The plane spacing equation for the hexagonal structure is [38]

$$\frac{1}{d^2} = \frac{4}{3}\left(\frac{h^2 + hk + k^2}{a^2}\right) + \frac{l^2}{c^2}. \qquad (2\text{-}2)$$

Combining Bragg's law ($\lambda = 2d\sin\theta$) with (2-2) yields :

$$\frac{1}{d^2} = \frac{4}{3}\left(\frac{h^2 + hk + k^2}{a^2}\right) + \frac{l^2}{c^2} = \frac{4\sin^2\theta}{\lambda^2}. \qquad (2\text{-}3)$$

Rearranging (2-3) gives

$$\sin^2\theta = \frac{\lambda^2}{4}\left\{\frac{4}{3}\left(\frac{h^2 + hk + k^2}{a^2}\right) + \frac{l^2}{c^2}\right\}, \qquad (2\text{-}4)$$

thus the lattice parameters can be estimated from eq. 2-4.

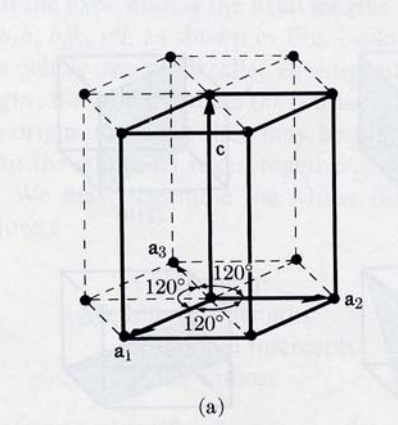

Fig. 2-4 The hexagonal unit cell

2.2.2 Rocking Curve

In Fig. 2-3 (b), fixed X-ray beam is incident upon the crystal. Crystal is then rotated ("rocked") through the Bragg angle θ, while the beam reflected by it is measured in a fixed detector with a wide slit. The resulting curve of intensity vs. θ is called a *rocking curve*. The width of a rocking curve is a direct measure of the range of orientation present in the irradiated area of the crystal, because each block (subgrain) of a typical mosaic crystal successively comes into reflecting position as the crystal is rotated.[38)]

2.3 PL Characterization

PL is very useful and powerful optical methods in the semiconductor industry, with its sensitive ability to find the emission mechanism and band structure of semiconductors. From PL spectrum the defect or impurity can also be found in the compound semiconductors, which affect materials quality and device performance. A given impurity produces a set of characteristic spectral features. The fingerprint identifies the impurity type, and often several different impurities can be seen in a single PL spectrum. In addition, the full width of half magnitude of each PL peak is an indication of sample's quality, although such analysis has not yet become highly

quantitative.[24)]

PL is the optical radiation emitted by a physical system (in excess the thermal equilibrium blackbody radiation) resulting from excitation to a nonequilibrium state by irradiation with light. Three processes can be distinguished: (i) creation of electron-hole pairs by absorption of the excited light, (ii) radiative recombination of electron-hole pairs, and (iii) escape of the recombination radiation from the sample. Since the excited light is absorbed in creating electron-pair pairs, the greatest excitation of the sample is near the surface; the resulting carrier distribution is both inhomogeneous and nonequilibrium. In attempting to regain homogeneity and equilibrium, the excess carriers will diffuse away from the surface while being depleted by both radiative and nonradiative recombination processes. Most of the excitation of the crystal is thereby restricted to a region within a diffusion length (or absorption length) of the illuminated surface. Consequently, the vast majority of PL experiments are arranged to examine the light emitted from the irradiated side of the samples. This is often called front surface PL.

2.3.1. Fundamental Transition

Since emission requires that the system be in a nonequilibrium condition, and some means of excitation is acting on the semiconductor to produce hole-electron pairs. We consider the fundamental transitions, those occurring at or near the band edges.

1. Free excitons

A free hole and a free electron as a pair of opposite charges experience a coulomb attraction. Hence the electron can orbit about the hole as a hydrogen-like atom. If the material is sufficiently pure, the electrons and holes pair into excitons which then recombine, emitting a narrow spectral line. In a direct-gap semiconductor, where momentum is conserved in a simple radiative transition, the

energy of the emitted photon is simply

$$h\nu = E_g - E_x$$

where E_g and E_x are the band gap and the exciton binding energy

2. Bound excitons:

Similar to the way that free carriers can be bound to (point-) defects, it is found that excitons can also be bound to defects. A free hole can combine with a neutral donor to form a positively charged excitonic ion. In this case, the electron bound to the donor still travels in a wide orbit about the donor. The associated hole which moves in the electrostatic field of the "fixed" dipole, determined by the instantaneous position of the electron, then also travels about this donor; for this reason, this complex is called a "bound exciton". An electron associated with a neutral acceptor is also a bound exciton. The binding energy of an exciton to a neutral donor (acceptor) is usually much smaller than the binding energy of an electron (hole) to the donor (acceptor).

3. Donor-Acceptor Pairs

Donors and acceptors can form pairs and act as stationary molecules imbedded in the host crystal. The coulomb interaction between a donor and an acceptor results in a lowering of their binding energies. In the donor-acceptor pair case it is convenient to consider only the separation between the donor and the acceptor level:

$$E_{pair} = E_g - (E_D + E_A) + \frac{q^2}{\varepsilon r} \qquad (2\text{-}5)$$

where r is the donor-acceptor pair separation, E_D and E_A are the respective ionization energies of the donor and the acceptor as isolated impurities.

4. Deep transitions

By deep transition we shall mean either the transition of an electron from the conduction band to an acceptor state or a transition from a donor to the valence band

in Fig. 2-5. Such transition emit a photon $h\nu=E_g - E_i$ for direct transitions and $h\nu=E_g - E_i - E_p$ if the transition is indirect and involves a phonon of energy E_p. Hence the deep transitions can be distinguished as (1) conduction-band-to-acceptor transition which produces an emission peak at $h\nu=E_g - E_A$, and (2) donor-to-valence-band transition which produces emission peak at the higher photon energy $h\nu=E_g - E_D$.

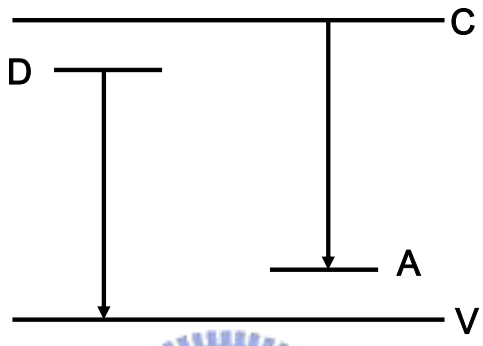

Fig. 2-5 Radiative transition between a band and an impurity state.

5. Transitions to deep levels

Some impurities have large ionization energies; therefore, they form deep levels in the energy gap. Raditive transitions between these states and the band edge emit at $h\nu=E_g - E_i$.[25)]

2.3.2 Influence of high excited light intensity[27)]

The PL conditions as shown before are excited by the low excitation light intensity. At low excitation light intensity (low density regime in Fig.2-6) the PL optical properties are determined by single electron-hole pairs, either in the exciton states or in the continuum. Higher excitation intensity (intermediate density regime in Fig.2-6) makes more excitons, such condition would lead to the **exciton inelastic scattering processes** and form the **biexciton**. The scattering processes may lead to a

collision-broadening of the exciton resonances and to the appearance of new luminescence bands, to and excitation-induced increase of absorption, to bleaching or to optical amplification, i.e., to gain or negative absorption depending on the excitation conditions. If we pump the sample even harder, we leave the intermediate and arrive at the high density regime in Fig.2-6, where the excitons lose their identity as individual quasiparticles and where a new collective phase is formed which is known as the **electron-hole plasma (EHP)**.

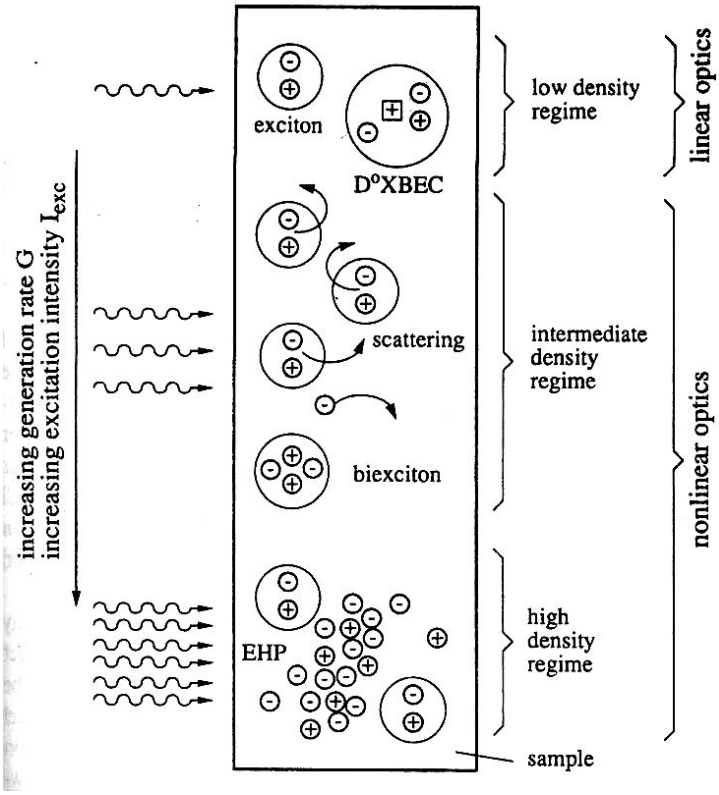

Fig. 2-6. The general scenario for many-particle effects in semiconductors[27)]

1. Scattering Processes

In the inelastic scattering processes, an exciton is scattered into a higher excited state, while another is scattered on the photon-like part of the polariton dispersion and leaves the sample with high probability as a luminescence photon, when this

photon-like particle hits the surface of the sample. This process is shown schematically in Fig.2-7 and the photons emit in such a process have energies E_n given by Ref. 28

$$E_n = E_{ex} - E_b^{ex}\left(1 - \frac{1}{n^2}\right) - \frac{3}{2}kT \qquad (2\text{-}6)$$

where n=2,3,4,…, E_b^{ex}=60meV is the binding energy of the free exciton in ZnO, and kT is the thermal energy. The resulting emission bands are usually called P-bands with an index given by n.

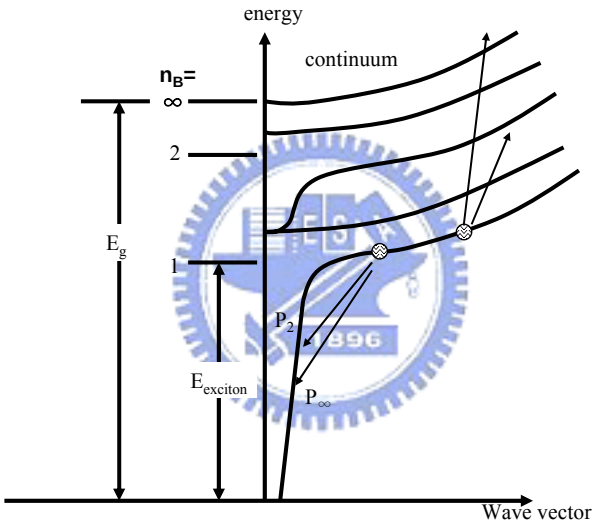

Fig.2-7. Schematic representation of the inelastic exciton-exciton scattering processes.[27)]

2. Electron-Hole Plasma

In this high density regime, the density of electron-hole pairs n_p is at least in parts of the excited volume so high that their average distance is comparable to or smaller than their Bohr radius, i.e., we reach a "critical density" n_p^c in an EHP, given to a first approximation by

$$a_B^3 n_p^c \approx 1$$

We can no longer say that a certain electron is bound to a certain hole; instead, we have the new collective EHP phase. The transition to an EHP is connected with very strong changes of the electronic excitations and the optical properties of semiconductors.

2.4 Raman scattering

When light passes through a medium, most of the light is reflected, transmitted, absorbed, elastic scattered, or inelastic scattered. Raman scattering is an inelastic scattering process. When the light encounters the medium, it interacts inelastically with phonon modes and produces outgoing photons whose frequencies are relatively shifted by an amount of energy correspondent to phonon energy from that of the incoming light. The scattered outgoing photons are called the Raman-scattered photons. If the light of frequency ν_0 is scattered by some media, the spectrum of the scattered light contains a strong line of frequency ν_0 and much weaker lines of frequencies $\nu_0 - \Delta\nu_1$, $\nu_0 - \Delta\nu_2$,……, $\nu_0 + \Delta\nu_2$, $\nu_0 + \Delta\nu_1$, etc. Those lines on the low frequency side of the exciting lines (i.e. $\nu_0 - \Delta\nu_i$,i=1,2,……) are always matched by lines on the high frequency side (i.e. $\nu_0 + \Delta\nu_i$,i=1,2,……) but the latter are much weaker when the scattering medium is at room temperature. Raman scattering is inherently a weak process, but laser provides enough intensity that the spectra can be routinely measured. In analogy with terms used in the discussion of fluorescence spectra, lines on the low frequency side of the exciting line are known as Stokes lines and those on the high frequency side as anti-Stokes lines.

The incident photon loses its energy by producing a phonon (Stokes shifted), or

gain energy and momentum by absorbing a phonon (anti-stokes shifted), according to the energy and momentum conservation rules:

$$h\nu_s = h\nu_i \pm h\Omega$$
$$q_s = q_i \pm K$$

where ν_i and ν_s are the incoming and scattered photon frequencies, q_i and q_s are the incoming and scattered photon wavevectors, Ω and K are the phonon frequency and wavevector, respectively.

All the Raman mode frequencies, intensities, line-shape, and line-width, as well as polarization behavior can be used to characterize the lattice and impurities. The intensity gives information on crystallinity. The line-width increases when a material is damaged or disordered, because damage or disorder occurs in a material will increase phonon damping rate or relax the rules for momentum conservation in Raman process. All these capabilities can be used as a judgment for layered microstructure as well as bulk materials, subject only to the limitation that the penetration depth of the exciting radiation range from a few hundred nanometers to few micrometers.

The E_2 mode of the wurzite ZnO crystal would shift to a higher frequency under the biaxial compressive stress within the c-axis oriented ZnO by the equation:

$$\Delta\omega(cm^{-1}) = 4.4\sigma(GPa)\ .^{29)} \qquad (2\text{-}7)$$

Where the $\Delta\omega$ is the frequency shift, and the σ is the stress in the biaxial direction of lattice.

2.5 SEM

The principle of the SEM, used for examining a solid specimen in the emissive mode, is closely comparable to that of a closed circuit TV system shown in Fig. 2-8. In the TV camera, light from the object forms an image on a special screen, and the

signal from the screen depends on the image intensity at the point being scanned. The signal is used to modulate the brightness of a cathode ray tube (CRT) display, and the original image is faithfully reproduced if (a) the camera and display raster are geometrically similar and exactly in time, and (b) the time for signal collection and processing is short compared with the time for the scan move from one picture point to the next.

In the SEM the object itself is scanned with the electron beam and the electrons emitted from the surface are collected and amplified to form the video signal. The emission varies from point to point on the specimen surface and so an image is obtained. Many different specimen properties cause variations in electron emission and so, although information might be obtained about all these properties, the images need interpreting with care. The resolving power of the instrument can not be smaller than the diameter of the electron probe scanning across the specimen surface, and a small probe is obtained by the demagnification of the image of an electron source by means of electron lenses. The lenses are probe forming rather than image forming, and the magnification of the SEM image is determined by the ratio of the sizes of raster scanned on the specimen surface and on the display screen.

For example, if the image on the CRT screen is 100 mm across, magnifications of 100X and 10000X are obtained by scanning areas on the specimen surface 1mm and 10μm across, respectively. One consequence is that high magnifications are easy to obtain with the SEM, while very low magnifications are difficult. This is because large angle deflections are required which imply wide bore scan coils and other problem parts, and it is more difficult to maintain scan linearity, spot focus and efficient electron collection at the extremes of the scan.

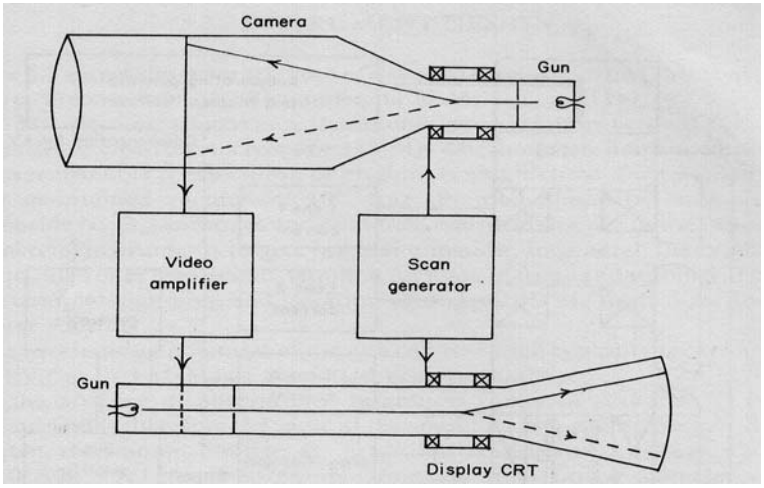

Fig.2-8 (a) Closed circuit TV

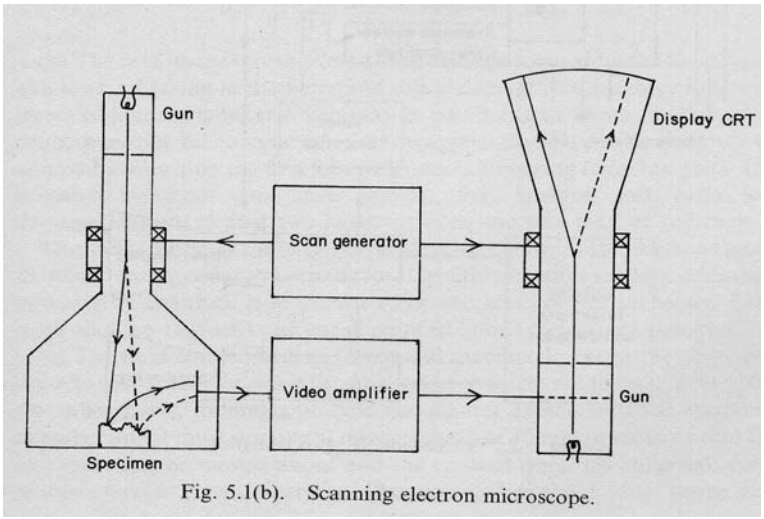

Fig.2-8 (b) Scanning electron microscope

2.6 Transmission electron microscopy (TEM)

TEM is an analytical imaging technique whereby a beam of electrons are focused onto a specimen causing an enlarged version to appear on a fluorescent screen or layer of photographic film. Like all matter, electrons have both wave and particle properties, and their wave-like properties mean that a beam of electrons can in some circumstances be made to behave like a beam of radiation. The wavelength is dependent on their energy, and so can can be tuned by adjustment of accelerating

fields, and can be much smaller than that of light , yet they can still interact with the sample due to their electrical charge. Electrons are generated by a process known as thermionic discharge in the same manner as the at the cathode in a cathode ray tube; they are then accelerated by an electric field and focussed by electrical and magnetic fields on to the sample. Details of a sample can be enhanced in light microscopy by the use of stains; similarly with electron microscopy, compounds of heavy metals such as lead or uranium can be used to selectively deposit heavy atoms in the sample and enhance structural detail, the dense electron clouds of the heavy atoms interacting strongly with the electron beam. The electrons can be detected using a photographic film, or fluorescent screen among other technologies. [39)]

Fig. 2-9 illustrates the principal results of electron scattering by a sample and, as a result, the principal sources of information that can be obtained. The operating modes are as follows: TEM, SEM, scanning transmission electron microscopy (STEM), and microanalysis (by X-ray and/or energy loss analysis or Auger analysis of surfaces).

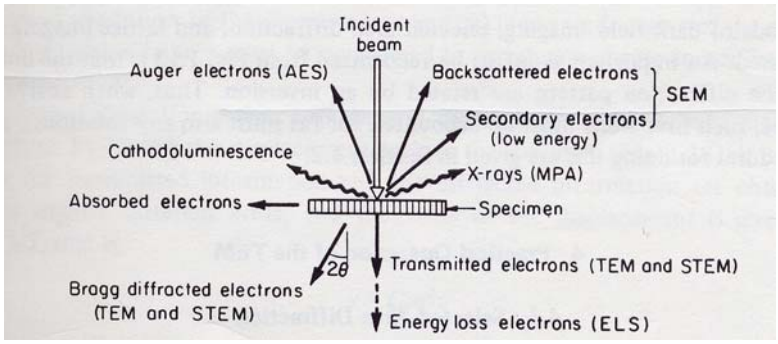

Fig. 2-9 Schematic showing electrons and electromagnetic waves emitted from a specimen as a result of elastic and inelastic scattering of the incident electron waves.

In the TEM mode, which is the one most often encountered, the microscope is operated Fig. 2-10 (a) to form images by bright field, dark field, or lattice image phasecontrast modes and Fig. 2-10 (b) to form idffraction patterns by using selected

area apertures and docusing the intermediate lens on the diffraction pattern formed in the back focal plane of the objective lens. Simple ray diagrams to illustrate these two modes are shown in Fig. 2-10. In the following sections the specially important methods of dark field imaging, selected area diffraction, and lattice imaging are discussed.

As the collimated beam of electrons passes through the crystalline specimen, it is scattered according to Bragg's law (eq. 2-1). The beams that are scattered at small angles to the transmitted beam are focused by the objective lens to form a diffraction pattern at its back focal plane (Fig. 2-10). When the intermediate and projector lens system is properly focused, a maginified image of the back focal plane of the objective lens will be projected on the viewing screen. An intermediate aperture may be inserted at the first intermediate image plane to limit the field from which the diffracted information is obtained. The intermediate selected area diffraction (SAD) aperture makes it possible to obtain diffraction patterns from small portions of the specimen. This technique is very useful, since a direct correlation can be readily made between the morphological and crystallographic information of very small areas. It is also necessary for establishing the diffracting and contrast conditions in the image. The technique is of particular importance when more than one phase is present in the specimen. [40)]

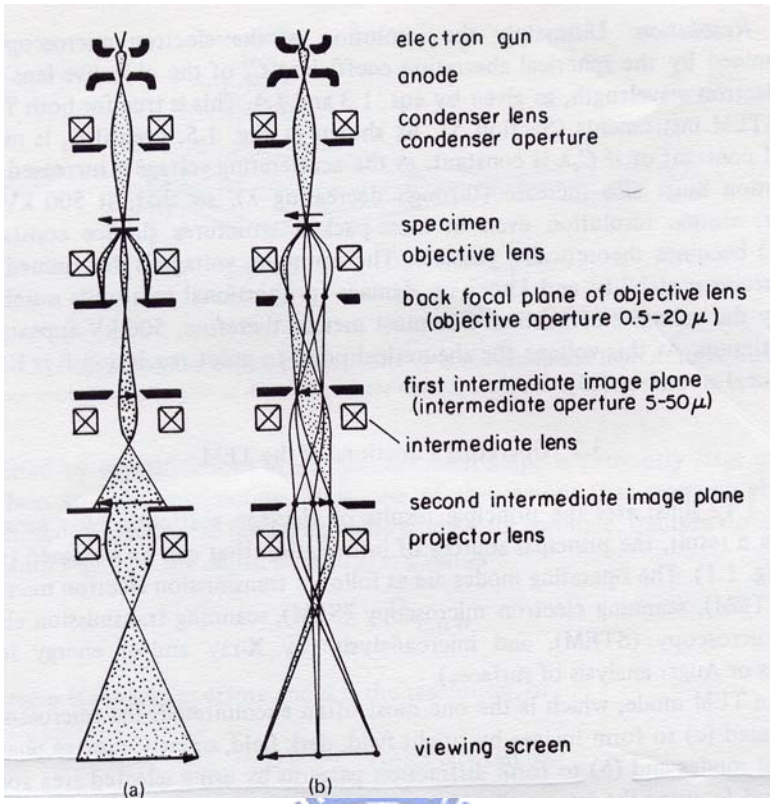

Fig. 2-10 Schematic ray diagram for a three-lens imaging microscope operated (a) for imaging and (b) for selected area diffraction.

Chapter 3 Experiment Process Detail

3.1 Sample Preparation

3.1.1 Surface treatment of the substrate

Amorphous quartz glass was used as the substrates for the growth of ZnO thin films. Before the surface treatment, the substrates were cut into a area of 20 ×10 mm^2 for the nanowires growth. Then these substrate were cleaned by using the following steps:

(1) Rinsed in D. I. water by a supersonic oscillator in 5 min.

(2) Rinsed in ACE (Acetone) solutions by a supersonic oscillator in 5 min.

(3) Rinsed in D.I water by a supersonic oscillator in 5 min.

(4) Dried with the gas of N_2.

After the surface treatment, the substrates were placed on the aluminum oxide boat filled with 1 gram of the Zn balls (99.999%, 6 mm in diameters) and ready to grow ZnO nanowires.

3.1.2 NiO thin film preparation

$Ni(NO_3)_2xH_2O$ was solved in the ethanol with concentration of 0.01M. The cleaned substrate was placed on the hot plate at 60℃ for 5 min. Then the $Ni(NO_3)_2xH_2O$/ethanol solution was sprayed onto this substrate by the sprayer. Then after baking for 5 min, the sample was ready for ZnO nanowires growth.

3.1.3 ZnO nanowires growth

The sample was placed on the alumina oxide boat filled with one gram of metal zinc balls. The vertical distance between the zinc source and the sample was about

3~5 mm. Then the alumina oxide boat which carried the sample was inserted into a quartz tube. This quartz tube was placed inside a furnace, with the center of the alumina oxide boat positioned at the center of the furnace and the substrates placed downstream of an argon flow (Fig.3-1). The quartz tube was kept 10-150 torr. The temperature of the furnace was ramped to 600^0C at a rate of 20-30^0C min^{-1} and then kept at that fixed temperature for 30 min under a constant flow of argon (50 sccm). After the furnace was cooled to the room temperature, dark gray-white material was obtained on the surface of the substrates.

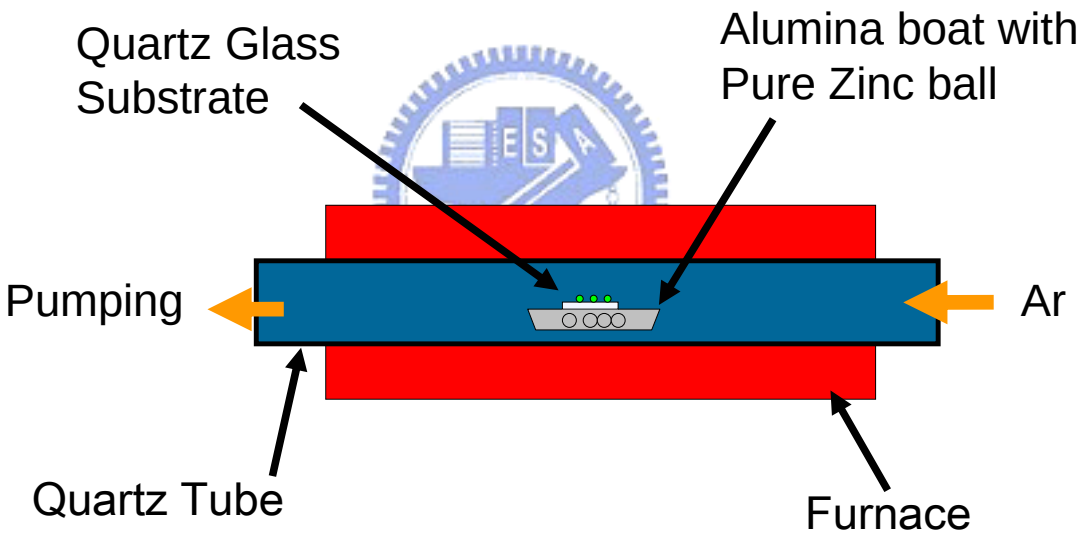

Fig. 3-1. Chemical vapor transport and condensation system

3.2 X-ray diffraction

After growing the ZnO nanowires, the crystal structures of the as-grown ZnO nanowires were inspected by X-ray diffractometer a JPN MAC Science MXP18 with a CuKα line (λ=1.5405 Å). The maximum voltage of the system is 30 kV with a maximum current 20 mA. The scanning step is 0.02^0 and scanning rate is 4^0 /min.

3.3 SEM system

The morphology of ZnO nanowires were observed by the Field Emission Gun Scanning Electron Microscopy (FEG-SEM)[Hitachi S-4000] The accelerated voltage is 0.5-30kV and the magnification is 20-300k times.

3.4 TEM system

The detailed structure of ZnO nanowires can be found by TEM. The TEM images were taken by Philips Tecnai-20 operated at 200 keV. The prepared nanowires were firstly suspended in alcohol by supersonic jolt and then the suspension was moved to the copper grid for observation.

3.5 PL system

A He-Cd laser (Kimmon IK5552R-F) operating at the 325 nm UV line is commonly utilized as a pumping source for PL. As shown in Fig. 3-2, the PL system includes reflection mirror, focusing and collecting lens, the sample holder and the cooling system. And a Nd:YAG Q-switched pulse laser (JDS uniphase CDRH PowerChip Nanolaser) operating at the 355 nm UV line,1 kHz , 500 ps, and 20 μJ per pulse is utilized as a high power pumping source for stimulated emission. As shown in

Fig. 3-3, this stimulated emission detection system includes the focus lens, the collecting fiber, and the sample holder.

In the two systems, we utilized two single-grating monochromators (TRIAX 320), one equipped with a CCD detector (CCD-3000), and the other equipped with a photo-multiplier tube (PMT-HVPS), which are matched with a photon counter for detection. The normal operated voltage of PMT is 0.8 kV. Moreover, we used a standard fluorescent lamps to calibrate our spectral response of spectrometer and detector. PL signals are exposed about 0.1 sec at a step of 0.1 nm, and the data are transmitted through a GPIB card and recorded by a computer. The monochromator is a 32 cm one with three selective resolutions of lines 600, 1200 and 1800 grooves/mm separately. When the entrance and exit slits are both opened to about 50 μm, the resolution is about 0.1 nm in this system. Low-temperature PL measurements were able to be carried out by using an additional closed cycle cryogenic system.

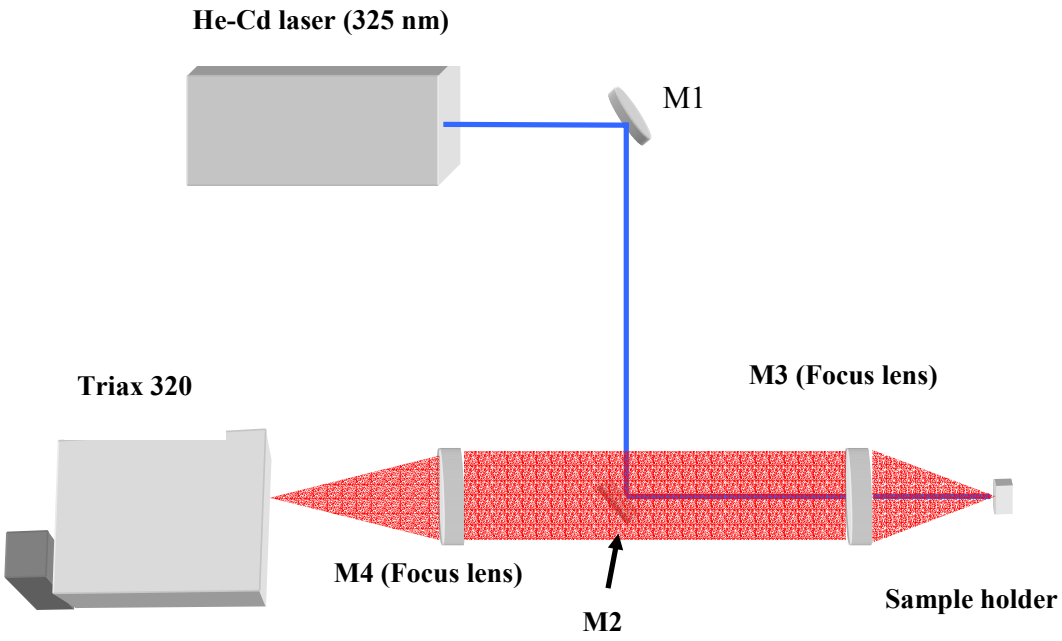

Fig. 3-2. PL system

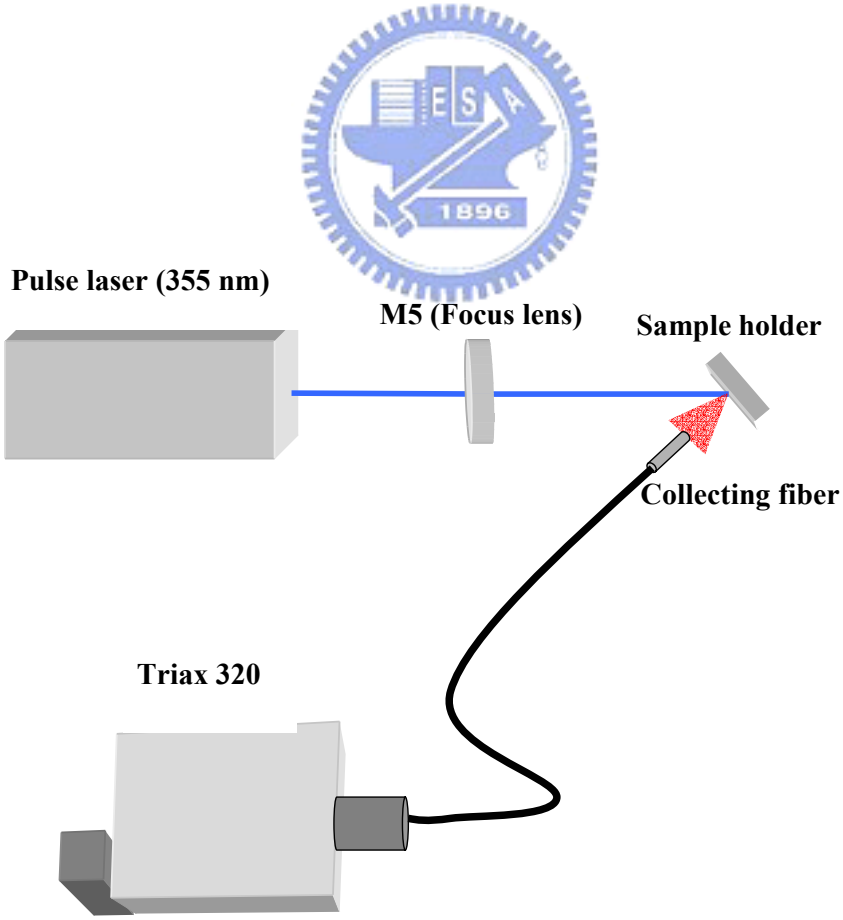

Fig. 3-3. Hihg power pumping PL system

Chapter 4 Results and Discussion

4.1 Growth of the ZnO nanowires

4.1.1 The growth mechanism of the ZnO nanowires

In the growing process the NiO particles on the substrate surface would attract the Zn and form ZnO. We sprayed the solution with very small $Ni(NO_3)_2xH_2O$ concentration of 10^{-5} M on the substrate and formed the very small pattern of NiO. After growing at the position far from the Zn source about 45 cm very small amount of ZnO formed on the substrate in Fig. 4-1. Obviously much more ZnO formed on the place with NiO particles than the place without NiO pattern. This result showed the function of the NiO is to attract the Zn and formed the ZnO.

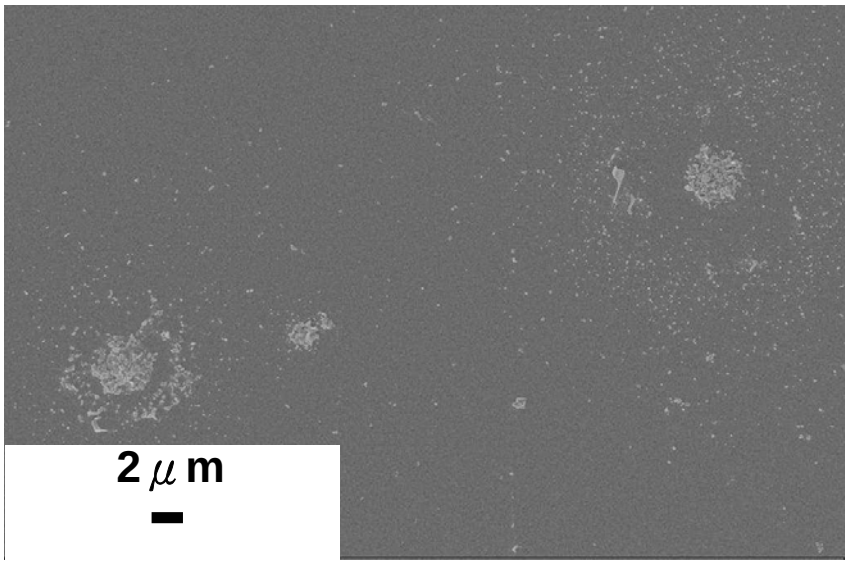

Fig.4-1. The ZnO attracted by the NiO pattern

We grew the ZnO nanowires on the substrate with NiO as shown in Fig. 4-2 (a) and without NiO, shown in Fig. 4-2 (b), at the same condition. The ZnO nanowires grown on the substrate with NiO particles were very well aligned, and the nanowires on the substrate without NiO particles showed a very disorder situation. This suggested that the NiO particles was constructive to the forming ZnO nanowires. It

was presumed that the NiO particles on the substrate help the nucleation of the ZnO and formed a buffer layer for growing well aligned ZnO nanowires.

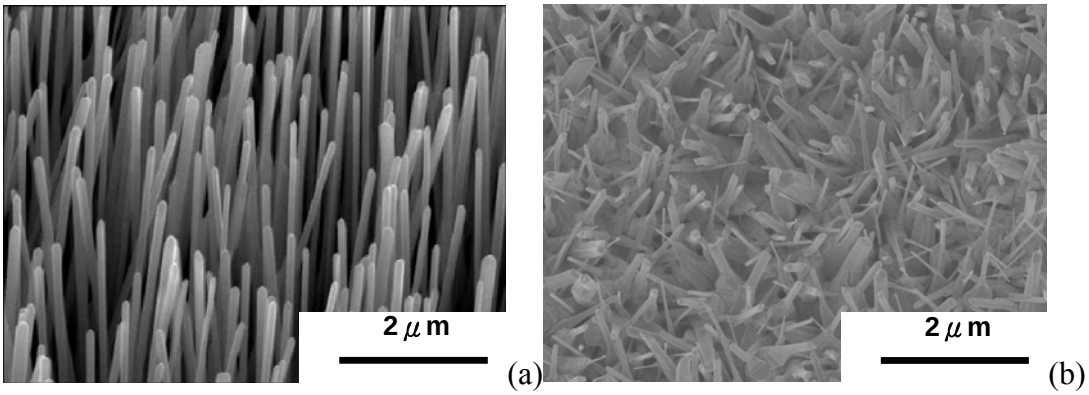

(a) (b)

Fig.4-2. The ZnO nanowires grown on the substrate with NiO (a), and grown on the substrate without NiO (b) in the same process: 50 torr, 550 ℃, 50 sccm Ar flow for 30 mins.

The well-orientation ZnO nanowires forming from the buffer layer on the substrate was observed in Fig. 4-3.

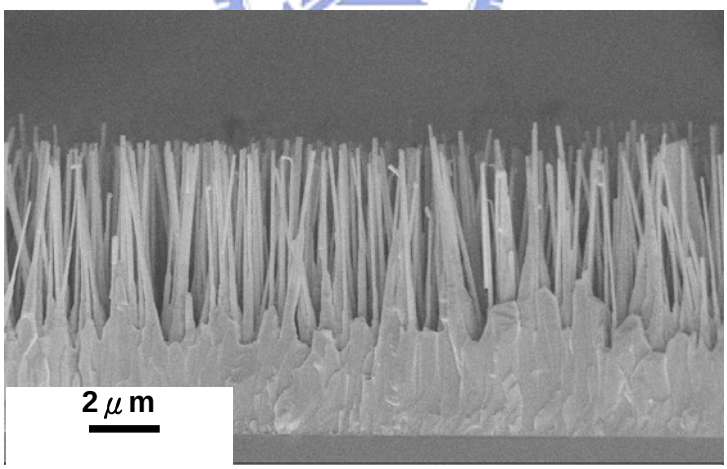

Fig. 4-3. The cross-section SEM image of the ZnO nanowires grown in the condition: 50 torr, 600 ℃, 50 sccm Ar flow for 30 mins.

This ZnO buffer-layer is considered the important key for the well alignment of the ZnO nanowires. This relation between the buffer-layer and the ZnO nanowires dominates the alignment of the nanowires.

The high quality ZnO epilayer (grown on sapphire by the Laser-MBE) was

taken as the substrate with a pre-grown ZnO buffer layer in order to identify the contribution of buffer layer to the alignment of the nanowires. After growing at the same process the sample was showed in Fig. 4-4. The ZnO nanowires grown on the high quality buffer layer have a very good orientation which reveals that the buffer-layer is an important key of the alignment of the nanowires.

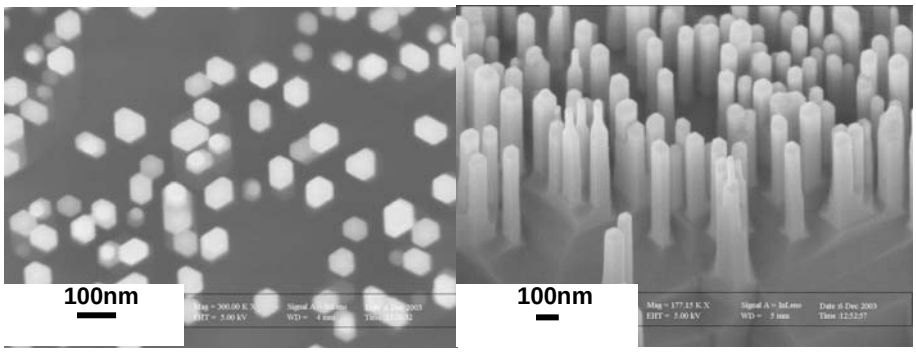

Fig. 4-4. The ZnO nanowires grown on the high quality ZnO thin film

The well aligned ZnO nanowires arrays were synthesized by the low temperature vapor deposition method which referred to Ref. 22. This method starts with the zinc balls vaporing at the suitable temperature and forms the Zn vapor which is deposited on the NiO particles on the substrate. A rough buffer-layer of ZnO form after ZnO grains form on the NiO particles through the Zn vapor deposition process. Then the ZnO nanowires start to grow on this ZnO buffer-layer with continual Zn vapor deposition. This formation of the ZnO nanowires through the physical vapor deposition process schematically illustrates in Fig. 4-5.

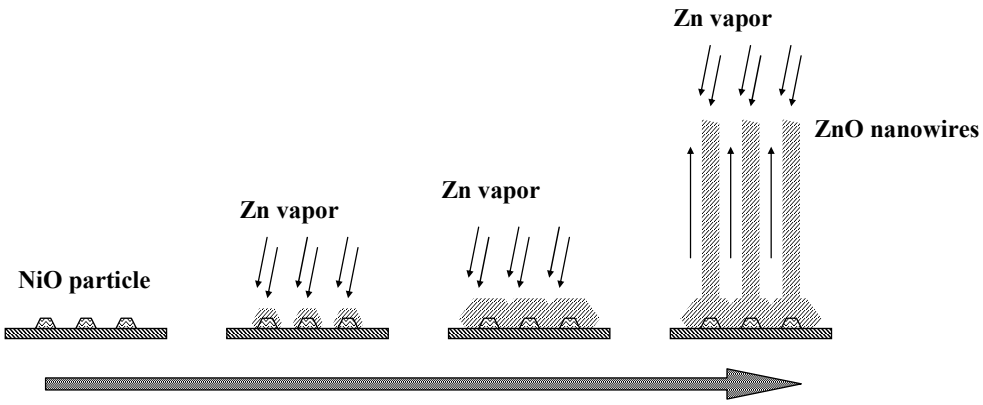

Fig. 4-5. The mechanism of growing ZnO nanowires

4.1.2 The influence of the ambient pressure

In this thesis we control the diameter of the ZnO nanowires by controlling the growth pressure. Inside the tube the gas flow condition is influenced by many parameters such as temperature, gas flowing velocity, and pressure. And the gas flowing condition can be classified as viscous flow region and molecular flow region according to the pressure. The gas flowing condition in the molecular flow region behaves like molecules move straight and collide with the tube and knock against the other molecules once in a while. The molecular flow region needs vacuum as high as 10^{-3} torr according to our instrument setup. Obviously the experiment process was operation under the viscous flow region at the lower vacuum region about 1 ~ 760 torr.

In the viscous flow region gas molecules will collide with each other frequently and flows like liquid flowing. The gas flowing conditions in the viscous flow region could be classified as laminar flow and turbulent flow (Fig. 4-6).

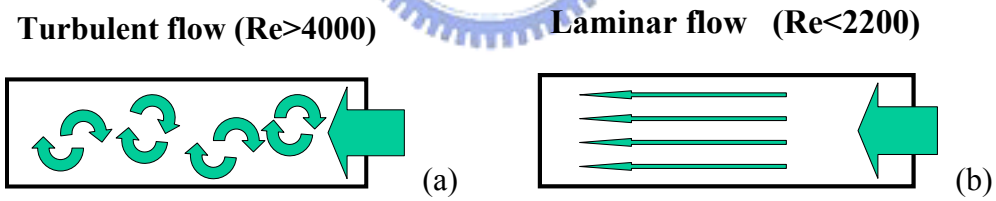

Fig.4-6. The sketch of turbulent gas flow condition (a), and laminar flow condition (b).

The gas in the laminar flow condition would flow smoothly along the tube direction such as Fig. 4-6(b). In turbulent flow condition the gas would also flow along the tube direction and additionally flow up and down turbulently as Fig. 4-6(a). These two flow conditions could be indicated by the Reynold number (Re):

$$\mathrm{Re} = \frac{Du\rho}{\mu} \qquad (4\text{-}1)$$

where D is the tube diameter, u is the flowing velocity of the gas, ρ is the gas density,

and μ is the gas viscosity. While the Re is large than 4000 the gas flows as turbulent flow, and less than 2200 flows as laminar flow. The gas flow would be transition condition while Re is between 2200 and 4000.

The Re number formula is defined at a very simple assumption with a straight and free-block tube. In our experiment there are some difficulties for calculating the Re number. First the gas flowing velocity is determined by the mass flow controller in front of the gas pipeline and changes at the tube connecting point with large diameter variation. Second there is a boat in the middle of the tube and creates a big complex structure for the gas flowing which would make the turbulent flow. We believe the turbulent flow would account for large growth pressure in our experiment.

4.1.3 The diameters of the ZnO nanowires

The size distribution and mean diameters of the ZnO nanowires were calculated from the SEM images by statistical counting. The typical size histograms[30] of the ZnO nanowires grown at 10 torr ~ 150 torr are depicted in Fig. 4-7(a~d). The standard deviations (Sd) of the size distribution were also calculated and shown with the mean diameters in Fig. 4-8. The Sd values and mean diameters increase as the growth pressure raised from about 100 to 150 torr. This result is attributed to the gas flow condition changed. The gas flow condition is predicted laminar flow under about 100 torr. In laminar gas flow the Zn particles flow smoothly along the tube without much lateral colliding which was responsible for the small mean diameter and Sd values. With the growth pressure increasing the gas started to flow turbulently and was followed by the lateral gas particles colliding. This gas behavior increases the opportunity of Zn particles falling on the substrate so that increases the ZnO nanowires mean diameters and Sd values.

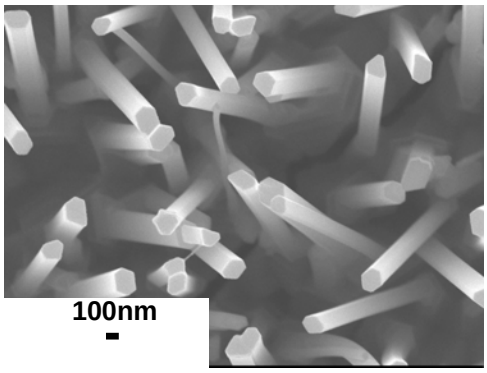

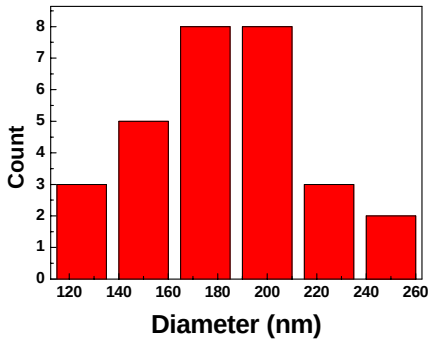

(a)

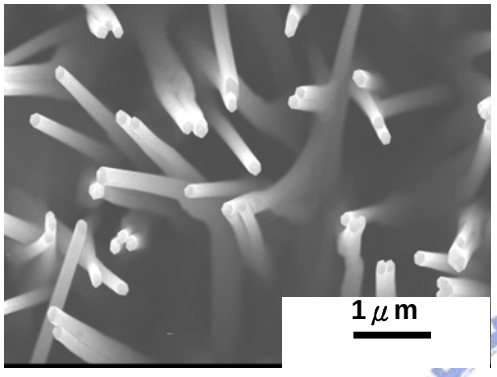

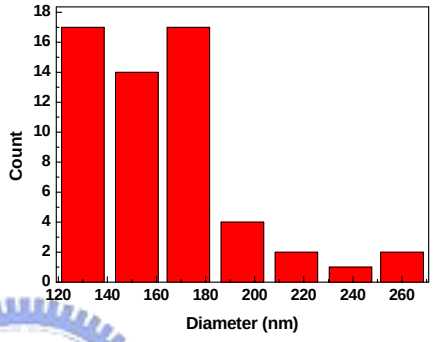

(b)

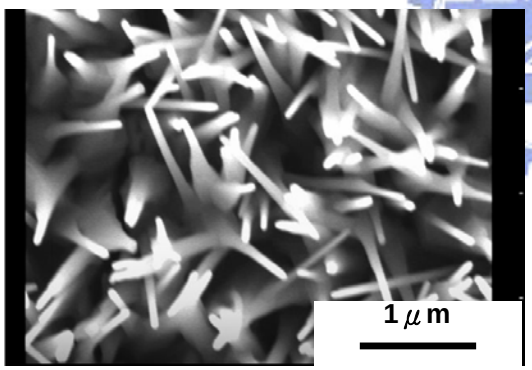

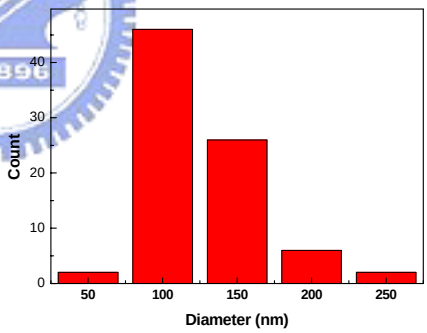

(c)

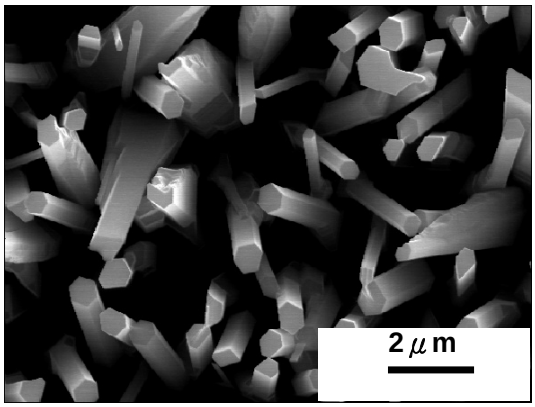

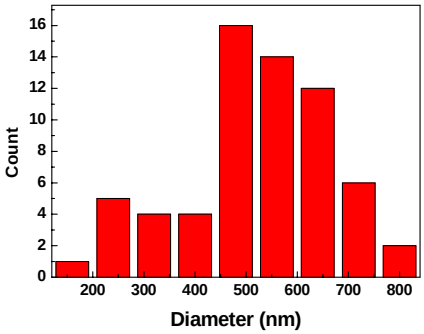

(d)

Fig. 4-7. The SEM images of the ZnO nanowires grown at 10 torr(a), 50 torr(b), 100 torr(c),and 150 torr(d) with the diameter dispersion diagrams.

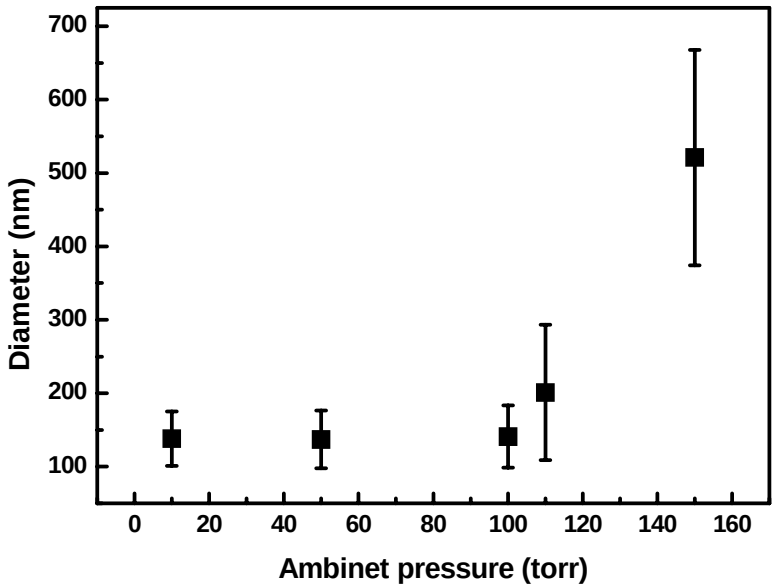

Fig. 4-8. The diagram of the diameters vs. ambient pressure.

4.2 Results of TEM

The detailed structure of individual ZnO nanowires have been characterized using transmission electron microscopy (TEM) and it's selected area diffraction (SAD) mode. The Fig. 4-9 provides direct evidence the single crystalline of the nanowires with the lattice fringes present. The SAD pattern inserted in Fig. 4-9 shows the electron diffraction pattern with the incident electron beam along $[\bar{1}2\bar{1}0]$ of the ZnO nanowires and indexed the reflection of wurtzite ZnO structure, which is consistent with the above XRD results.[50] The TEM image and SAD pattern confirm that the nanowires grow along the c-axis direction, which is in consistent with the above XRD results.

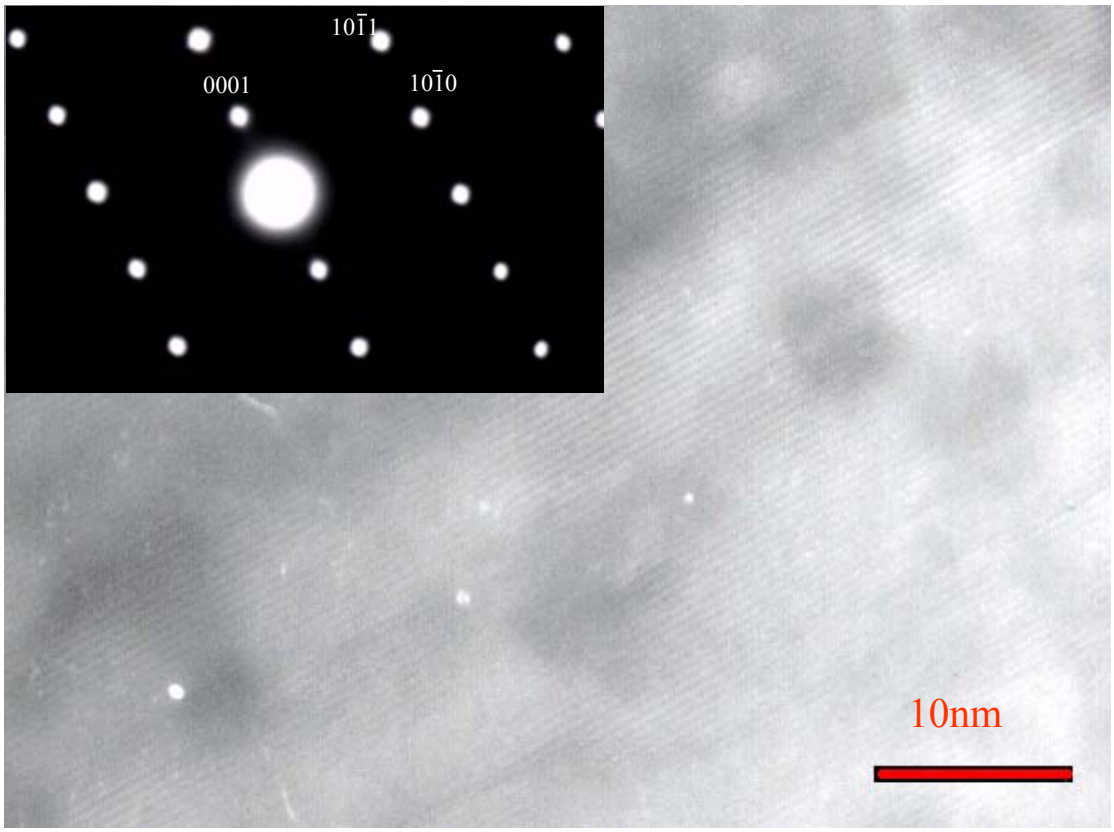

Fig. 4-9. TEM image of a nanowire. The insert of Fig. 4-8 is the SAD pattern.

4.3 Result of the X-ray diffraction measurement

Fig. 4-10(a) presents the XRD pattern of the nanowires grown at 600℃ under 150 torr tube pressure for 30 mins. The strongest peak at 34.5° and two relatively small peaks at 31.58 and 36.1° were observed for (002), (100), and (101) crystal planes, respectively. These peaks can be indexed to a hexagonal structure of ZnO with cell constants of a = 3.269Å and c = 5.195 Å by eq. 2-4 that reveals good single crystalline as compared with the bulk ZnO (a=3.249Å, c=5.206Å, according to JCPD-36-1451). According to the Scherrer formula :[38)]

$$t = \frac{0.9\lambda}{B\cos\theta_B}$$

the size of the single crystal grain inside the nanowires could be estimated. Where the λ is X-ray wavelength, B is the full width at half maximum (FWHM) of the peak at θ_B which is the diffraction peak. Substitute the $\lambda = 1.5405$ Å, B=3.46X10^{-3} radian, and $\theta_B = 17.22^o$. The t value would be about 421Å which means that the crystal grain was about 421 Å thick.

However, the rocking curve (see Fig. 4-10(b)) of the nanowires shows the FWHM of 10.079°. The broad diffraction peak may be a result of an angle distribution of the nanowires oriented $\pm 5^o$ around the <002> direction.

4.4 Result of the Raman scattering

The typical Raman spectra of the ZnO nanowires grown on silicon substrate is shown in Fig. 4-11. The observed phonon frequencies are E_2(high) = 435.96 cm^{-1}, A_1(TO) = ~378 cm^{-1}. The present of the A_1(LO) = ~580cm^{-1} associated with lattice defect, such as oxygen vacancies and zinc interstitial in the ZnO nanowires, is similar to the results of Ref. 35 Clearly, this result indicates that the sample is composed of ZnO with few defect in the nanowires. As displayed in Fig. 4-11, the E_2 mode of the

ZnO nanowires shift to a lower frequence under the biaxial tensile stress within the ZnO nanowires as predicted by equation (2-7). The frequency of the E_2 mode observed in the nanowires was 435.96 cm^{-1} lower than 437 cm^{-1} which was observed in the bulk ZnO crystal. The E_2 mode shift of the ZnO nanowires grown on the quartz glass substrate were under tensile stress 0.236GPa. The stress could be induced by the interface of the buffer-layer and the quartz glass substrate with different thermal expansion coefficient. The ZnO buffer-layer and nanowires are formed at high temperature 600℃, and cooled down to room temperature. The ZnO with larger thermal expansion coefficient of $4.8x10^{-6}K^{-1}$ would result in the larger difference of lattice and quartz glass with smaller expansion coefficient of $0.51x10^{-6}$ K^{-1} would produce the tensile stress on the ZnO buffer layer while cooling down to room temperature from growth temperature. This result agrees with the phenomenon of the XRD measurement.

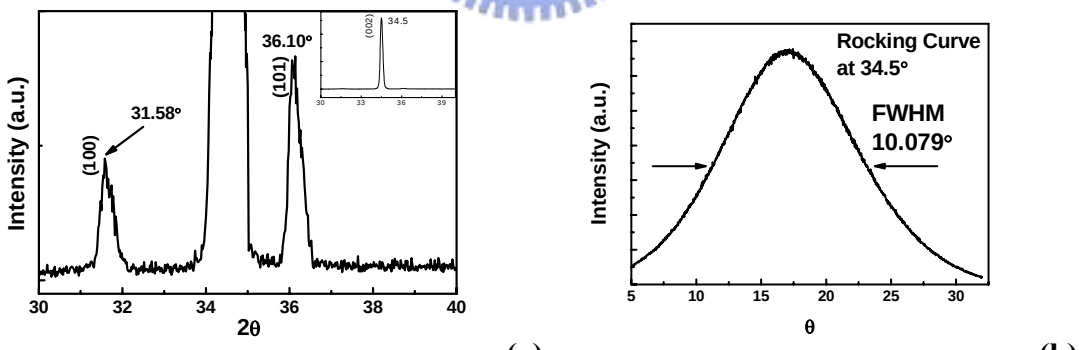

Fig. 4-10. The ω-2θ XRD pattern (a) and rocking curve (b) of the ZnO nanowires grown at 50 torr, 600 ℃, 50 sccm, 30 mins.

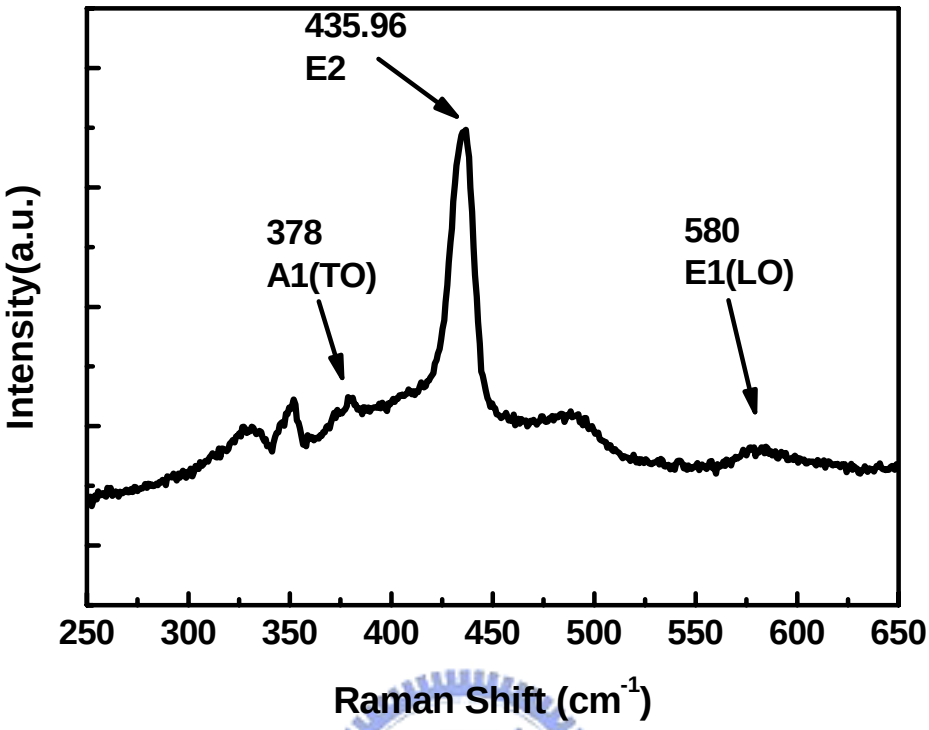

Fig. 4-11. The Raman spectrum of the ZnO nanowires. grown at 50torr, 600℃, 50sccm, 30mins.

4.5 PL spectra of ZnO nanowires

4.5.1 Room-Temperature

In the room-temperature PL spectra the quality of the ZnO nanowires were examined. The diameters of the nanowires increase with the growth pressure but the quality degrades. In Fig. 4-12(a) the room temperature PL of samples of different growth pressure shows that the peak positions also change with the growth pressure. The peak position at 3.25 eV doesn't change under 100 torr of growth pressure and then red-shiftes to 3.22 eV over 100 torr, and the full-width half-maximum(FWHM) of these peaks raises as the growth pressure increasing. (Fig. 4-12(b)) From the broad band defect emission at about 2.54 eV the intensity of the sample grown over 100 torr are larger than the sample grown under 100 torr. Such a result indicates higher defects and impurity concentration in the nanowires with growth pressure larger than 100 torr. The defect and impurity concentration could be resulted from the turbulent flow which made the Zn or ZnO particles to strike the growing ZnO nanowires. Then the defect and impurity resulted in donor-acceptor pair(D^0A^0) in the material provide and lead to the larger PL of D^0A^0 emission. At room-temperature the D^0A^0 would turn into free electron-acceptor transitions (eA^0) because the donors are thermally ionized.[31] The eA^0 emission at about 3.22 eV overlaps with the free exciton at about the 3.31 eV and made the peak move from 3.25 to 3.22 eV .[32]

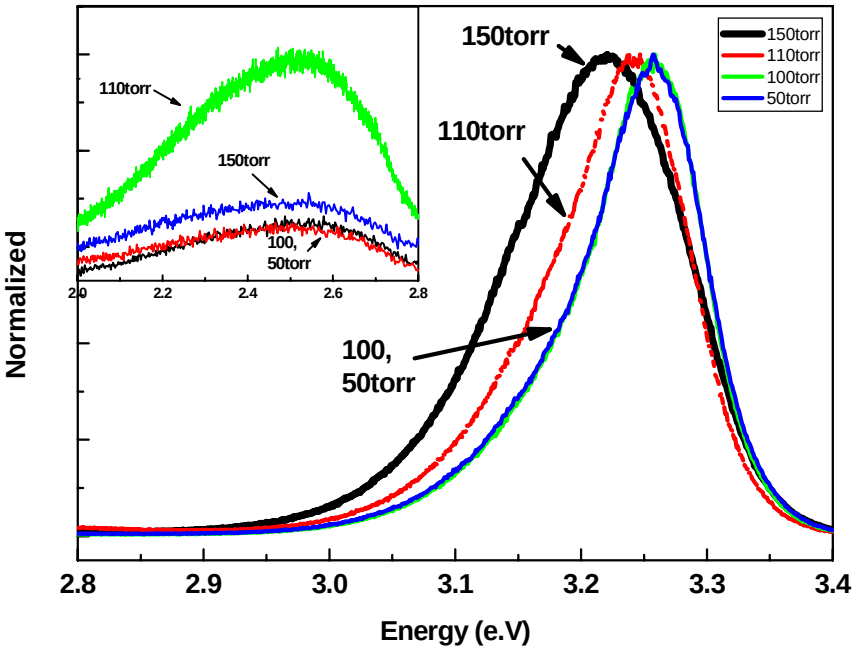

(a)

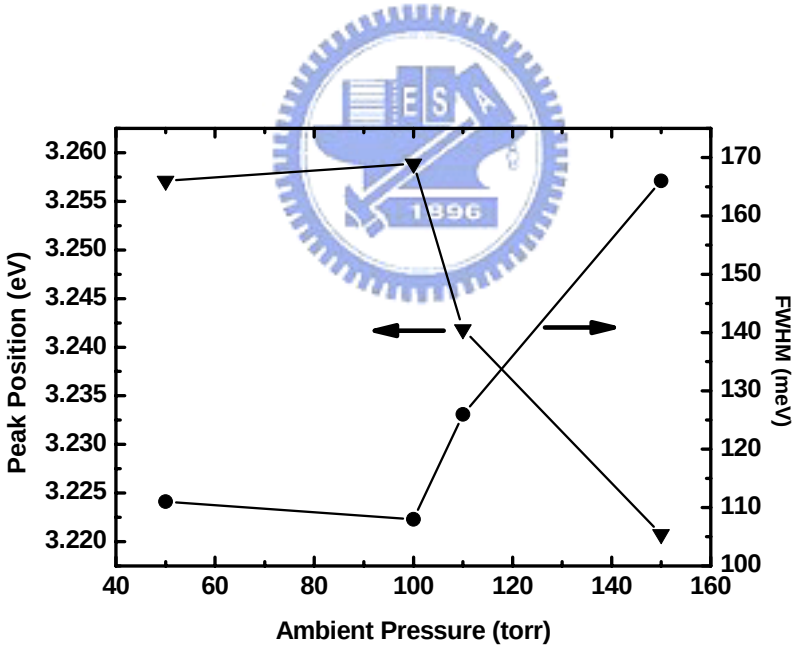

(b)

Fig. 4-12. The room temperature PL (a) and variation of the full-width half-maximum peak position (b) of the ZnO nanowires grown from 50~150 torr.

4.5.2 Temperature and Power dependent PL

Fig. 4-13(a) is the temperature-dependence PL at the temperature from 12 K ~ 300 K. We observed that the emission peak at 3.366, 3.369 and 3.373 eV decrease as temperature increases but the shoulder at 3.382 eV increases. This behavior presumably results from decomposition of bound excitons due to the increasing thermal energy, and hence supports the argument that the PL corresponds to a free exciton peak (EX) and the others to bound exciton peaks (D^0X, D^0X1, A^0X). Above 60 K, the intensities of the exciton recombination peaks also show a decrease with increasing temperature because of thermally induced dissociation of electron-hole pairs. However, the EX peak extends to room temperature, in contrast to those of the two bound ones disappearing around 150 K.

Then we perform numerical analyses of the energy position of the EX as function of temperature using a model which is a modification of the Varshin equation for temperature dependence of band gap:

$$E(T) = E(0) - \frac{\alpha T^2}{\beta + T} \qquad (4\text{-}2)$$

We obtain the band gap of ZnO by fitting to the above equation to be 3.384 eV see [Fig. 4-13(b)]. It is similar to energy band gap (E_0 = 3.380 eV) obtained by C. Boemare et al.[33)]

The low temperature (12K) PL spectrum of different pumping power density is presented in Fig. 4-13. It shows that the EX and bound exciton peaks do not changed with increasing power density. Besides, we observed two intensity peaks at 3.316 and 3.242 eV increase as the EX intensity increases in Fig. 4-14(a) once the the temperature raises above 90K that corresponding to the phonon replicas.[34)] The peak at 3.225 eV slightly blue-shifted with increasing pump intensity. It is due to the number of occupied donor and acceptor centers and this decreasing the average

separation of the pair center. As a consequence one finds that the emission maximum of the pair-band shifts to the blue with increasing excitation due to the Coulomb term in the function of donor-acceptor pair described in Chapter 3. This is a characteristic feature of donor-acceptor pair recombination.

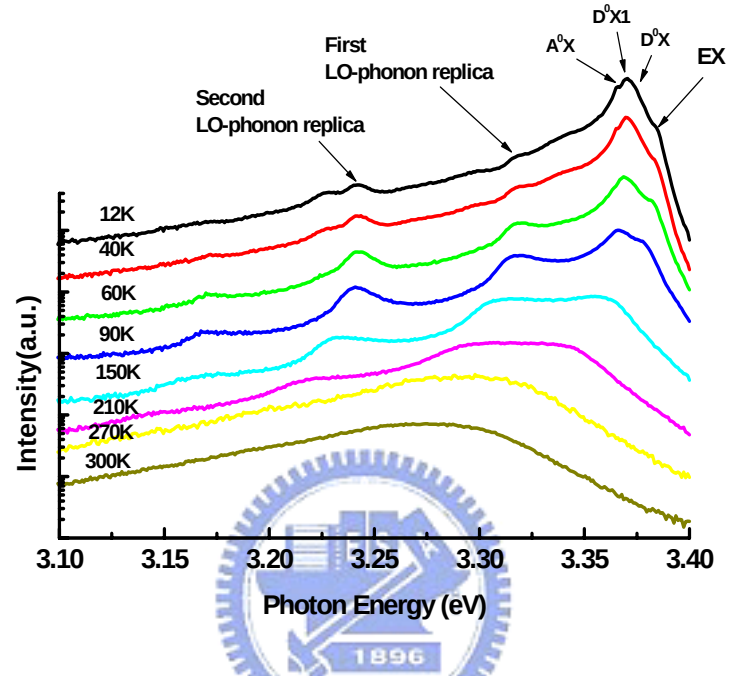

(a)

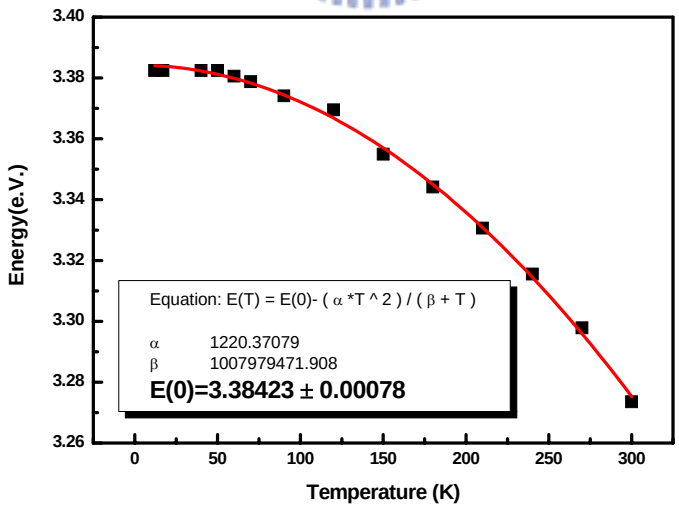

(b)

Fig. 4-13. The temperature dependence PL of the ZnO nanowires (a). Temperature dependences of the free exciton of ZnO nanowires with theoretical fitting curve (b).

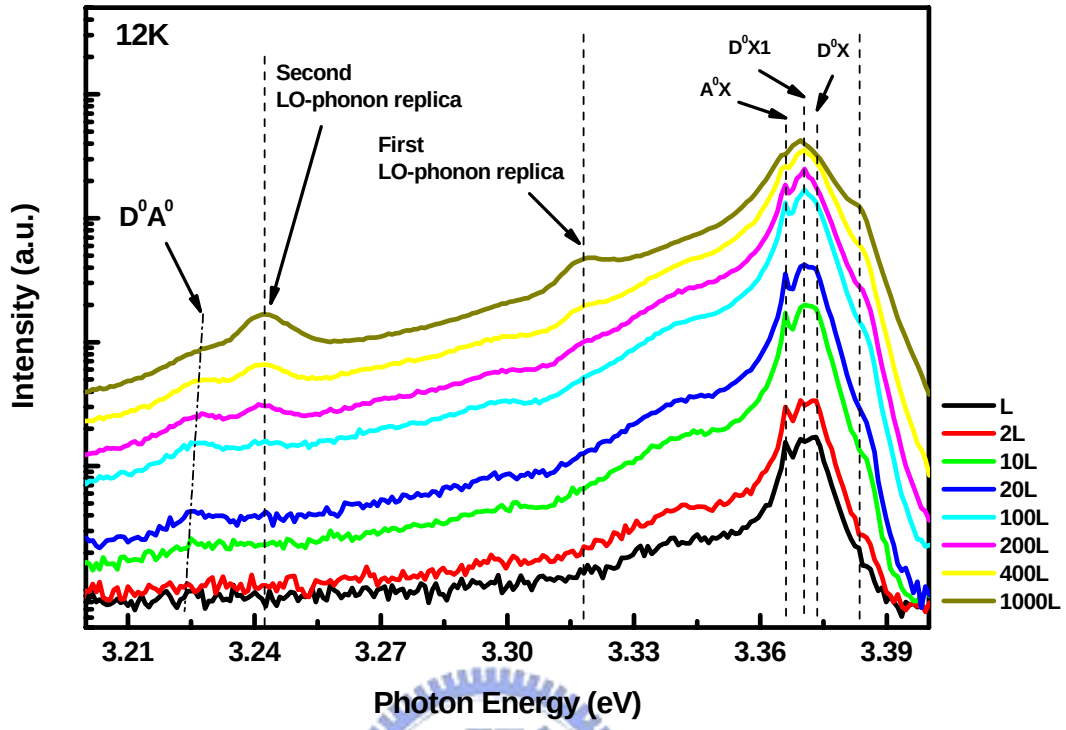

Fig. 4-14. The low temperature power density dependence PL spectrum of the ZnO nanowires.

4.5.3 High pumping power density

The emission signals were collected in a back scattering configuration. Fig 4-15 shows the emission spectrum at room temperature obtained at different excitation intensities. At extreme low pumping, the observed emission spectrum is similar with the spontaneous emission with peak position around 3.22 eV. With increasing pump intensity, the free exciton would be scattered to the lower energy levels (E_n) which follows the relation eq. 2-6. We observed a new band designated as P_2 immediately appears at photon energy lower than the main peak and another peak P_∞ appears at even higher pumping.

The P_∞ band at 3.188 eV lies 17 meV below the P_2 band is approximately equal to 15 meV which is the difference between n = ∞ and n = 2 estimated from Eq. 2-6. And the peak positions of P_∞ and P_2 bands are independent of the pumping intensity. At considerable higher pumping power, the stimulated emission peak abruptly red-shifts due to formation of electron-hole plasma (EHP).

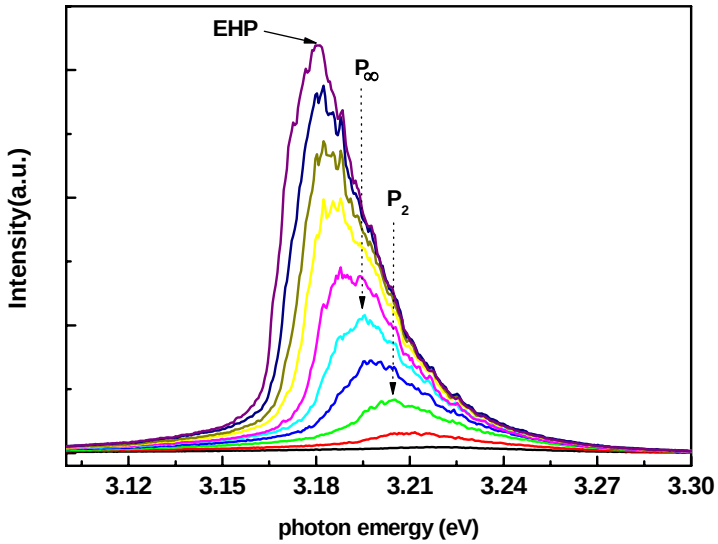

Fig. 4-15. The valued high pumping power density spectrum of the ZnO nanowires at room temperature .

Chapter 5 Conclusion and future work

5.1 Conclusion

The single crystal ZnO nanowires were successfully grown on the amorphous quartz substrate by simple vapor deposition method. The diameters of the nanowires can be controlled through tuning the ambient growth pressure. The flow condition would change from laminar flow to turbulent flow at the critical ambient pressure about 100 torr which is the reason for larger diameters of the nanowires.

According to the XRD patterns the nanowires were wurtzite structure and grew along the c-axis. The XRD and Raman spectrum indicate that the a-axis suffered the tensile stress and lead to the c-axis. The TEM image and SAD pattern show the single crystalline of the nanowires is stress within the nanowires. The SEM images show the nanowires with diameters about 100~500 nm and about 4 μm in length, and the nanowires are grown on top of a 2μm thickness buffer layer.

The room temperature PL spectrum of the nanowires consists of UV emission band at 3.25 eV. From the RT-PL analysis, we found that the UV emission band red-shifted to 3.22 eV with larger diameter nanowires of worse. Through the temperature dependent PL the band gap of 3.382 eV was obtained. The low-temperature power dependent PL spectrum displayed the donor-bound exciton, acceptor-bound exciton, donor-acceptor pairs, and free exciton with several LO-phonon replicas. Under high pumping power density, the exciton-exciton collision dominates the emission with peaks at 3.1956 and 3.2048 eV (P_∞ and P_2), and under even higher pumping, the EHP recombination processes takes over and dominates the emission at 3.18eV.

5.2 Future work

In many measurements the data is not enough to clearly distinguish the influence of the buffer layer and the nanowires, and this is an important issue for the development of the ZnO nanowires. In the future the properties of the ZnO nanowires and buffer layer would be identified separately. Further the research on the influence of nanowire structure, such as diameter and length, upon the optical properties, such as PL, Raman, and stimulated emission spectrum, would be carried out. Then the potential of making nano-optical-device by employing the ZnO nanowires would be investigated.